Supplementary Information (SI) for Nanoscale.
This journal is © The Royal Society of Chemistry 2026

Supporting Information

Type-II WO_3/NiOOH Nanoflakes Enable Efficient and Selective Low-bias Photoelectrochemical Saline Water-Splitting Reaction

Prashant Choubey,[1] Shiyanshi Nuwal,[1] Mrinmoyee Basu[1]*

[1]Department of Chemistry, BITS Pilani, Pilani Campus, Rajasthan-333031

Email: mrinmoyee.basu@gmail.com

Materials: Tungstic acid from SRL, Nickel nitrate hexahydrate from SRL, sodium nitrate from molychem, Potassium chloride from SRL, urea 99% extrapure from loba chemie, oxalic acid extrapure(99.5%) from SRL, hydrogen peroxide (30%) from merck, miliQ water, concentrated HCl (35%) from merck, acetonitrile (HPLC grade) from spectrochem, ethylene diamine from merck, ammonia solution (25 wt%) from merck and Fluorine-doped tin oxide coated glass (FTO, 1 × 1 cm^2, resistivity 10 Ω/square, thickness 5 mm) was purchased from Sigma-Aldrich.

Characterizations: Shimadzu spectrophotometer (model no. UV-2450) with a deuterium and tungsten-halogen lamp is used to study ultra-violate visible spectroscopy. Thin film X-ray analysis is carried out using Bruker D2 phaser X ray diffractometer with incident radiation of Cu-Kα. The entire analysis is conducted at a scanning rate of 2° per minute. Microscope version, XT Platform version, XT UI version, Modal- "APREO S" FE-SEM is used to investigate the morphology of the synthesized WO_3, and WO_3/NiOOH. EDS analysis is carried out for these samples using the EDS attachment with FESEM, which is Aztec (software), X-MaxN, NS: 77887 (Detector) of the Oxford company. Steady state fluorescence spectra of WO_3 and WO_3/NiOOH are done by FluoroMax spectrofluorometer of Horiba. The FTIR spectra are obtained using a Shimadzu IR Affinity-1S spectrometer. Raman analysis is carried out using the HORIBASCI Raman instrument (model no LabRAM HR EVO). TEM and HRTEM analysis are carried out using the TALOS F200S G2 HRTEM (Acceleration voltage of 80 and 200kV). XPS analysis is carried out by a ThermoFisher Scientific instrument in an ultra-high vacuum chamber ($7*10^{-9}$ torr) using Al-Kα radiation.

Photoelectrochemical Measurement: In this present case, photoelectrochemical study was conducted in a three-electrode system. PEC water splitting was carried out at 3.5 wt% NaCl as the electrolyte. In the cell Ag/AgCl electrode was applied as the reference electrode, Pt wire was used as the counter electrode and sample deposited FTO was used as the working electrode. A xenon lamp was used to illuminate the PEC cell with a fixed light intensity of 100 mW/cm^2. CH Instrument (CHI604E) was used to record all the photoelectrochemical data at 25 °C. The photoelectrochemical study was carried out using synthesized WO_3, and WO_3/NiOOH photoanodes upon applied potential from -0.2 to 1.2 V vs. Ag/AgCl keeping scan rate 50

mV/sec. 'i-t' amperometry study was carried out under the potential of '0.8'V vs. Ag/AgCl. Incident photon-to-current conversion efficiency is calculated by using the monochromator.

Photoelectrochemical Impedance Study:
Photoelectrochemical impedance measurement was also performed in a three-electrode system. It was performed with the sweeping of frequency from 50 kHz to 1 Hz. A xenon lamp was used to illuminate the PEC cell with a fixed light intensity of 100 mW/cm^2.

Carrier lifetime:

Photocurrent transient dynamics were quantitatively determined by the I–t plot. To evaluate the recombination behavior of charge carriers over the photoelectrode through introducing a normalized parameter (D)

$$D=(It-Ist)/(Iin-Ist) \text{ --------(Equation 1)}$$

where It, Ist, and Iin correspond to the time-dependent, steady-state, and initial photocurrents, respectively. The transient time (τd) is defined as the time when ln D is equal to −1 which uncovers the general charge recombination behavior and charge lifetime.

Calculation of (ABPE) efficiency (η%): It is calculated with the help of the J-V plot and the following equation is used: $\eta = [J\ (1.23-V_{RHE})/Pin]$ %---------(Equation 2)

where J is the photocurrent density, V_{RHE} is the applied potential with respect to RHE, and Pin is the incident light intensity.

Incident-photon-to-current-conversion efficiency (IPCE): IPCE is measured by following equation: $IPCE = ((1240 \times J) *100)/ (\lambda \times I_0)$ --------(Equation 3)

Here, J is the photocurrent density (mA/cm^2), λ is the incident wavelength, and the I_0 is the incident light intensity (mW/cm^2).

Carrier-separation efficiency and charge injection efficiency: Photocurrent density in PEC system is given by following equation:

$$J_{PEC} = J_{abs} \text{ x } \eta_{sep} \text{ x } \eta_{inj} \text{ --------(Equation 4)}$$

Charge injection efficiency (η_{inj}) is calculated using the equation:

$$\eta_{inj} = J_{PEC}/J_{\text{Hole scavenger}} \text{ --------(Equation 5)}$$

where, $J_{\text{Hole scavenger}}$ is the observed photocurrent density in presence of hole scavenger.

Carrier transfer lifetime:

The carrier transfer lifetime (Γ_B) has been calculated according to the following equation:

$$\Gamma_B=(k_BT/e)\ [(d(OCP)/dt)^{-1}] \text{ --------(Equation 6)}$$

where k_B is the Boltzmann's constant, T is the temperature in K and e is the charge of single electron.

Supporting Information

Carrier density and the flat band potentials:

These are calculated by using the following equation:

$$1/Cs^2 = (2/e\varepsilon\varepsilon_0 N_d A^2)\,[(V - V_{FB} - kT/e)] \text{ -------(Equation 7)}$$

where Cs, e, ε_0, ε, N_d, V_{FB}, A, T, and k are specific capacitance, electron's charge, the electric permittivity of vacuum, the dielectric constant of the semiconductor, carrier density, flat band potential, area of the sample, temperature, and Boltzmann constant, respectively.

Photoelectrochemical Impedance Study:

Photoelectrochemical impedance measurement was also performed in a three-electrode system. It was performed with the sweeping of frequency from 50 kHz to 1 Hz. A xenon lamp was used to illuminate the PEC cell with a fixed light intensity of 100 mW/cm^2.

Calculation of Band Edge Position:

For calculation of band edge positions of WO_3 and NiOOH following equation are used:

$$\phi\ WO_3 + (E_f - VBM) = E_{VB};\ \text{--------(Equation 8)}$$

$$E_{CB} = E_{VB} + E_g,\ \text{--------(Equation 9)}$$

where ϕ = work function of the semiconductor, E_f is fermi energy level, VBM is valence band maximum, E_g is bandgap, E_{VB} and E_{CB} is band edge position of valance band and conduction band, respectively.

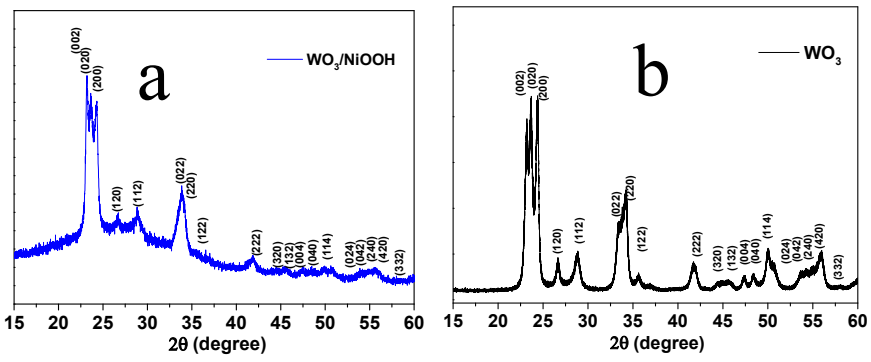

Figure S1: XRD patterns of (a) WO_3/NiOOH and (b) WO_3

Supporting Information

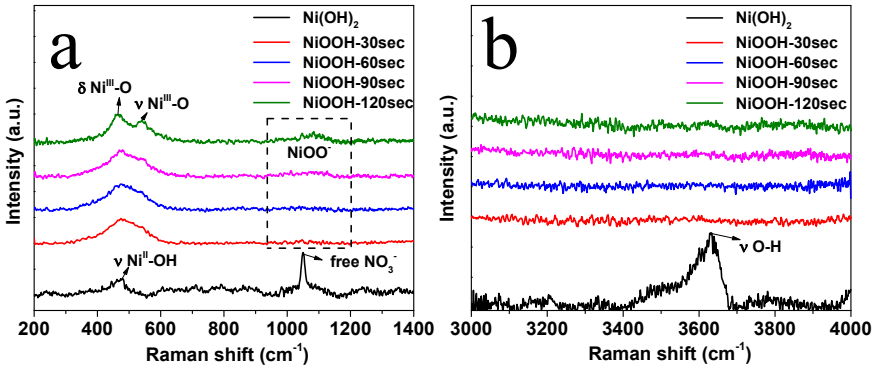

Figure S2: Raman spectra from(a) 200 to 1400 cm^{-1} and (b) 3000 to 4000 cm^{-1} Raman shift range of $Ni(OH)_2$ and its subsequent transformation to NiOOH after different amperometry (i-t) timings at 1.5 V vs. Ag/AgCl.

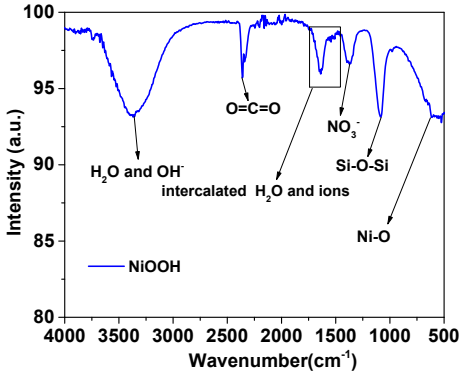

Figure S3: FTIR spectra from bare NiOOH on FTO.

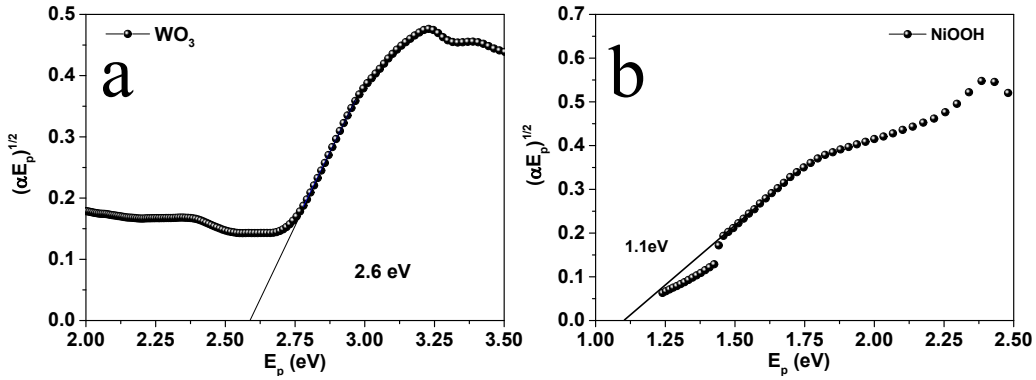

Figure S4: Tauc's plot of (a) WO_3, and (b) NiOOH.

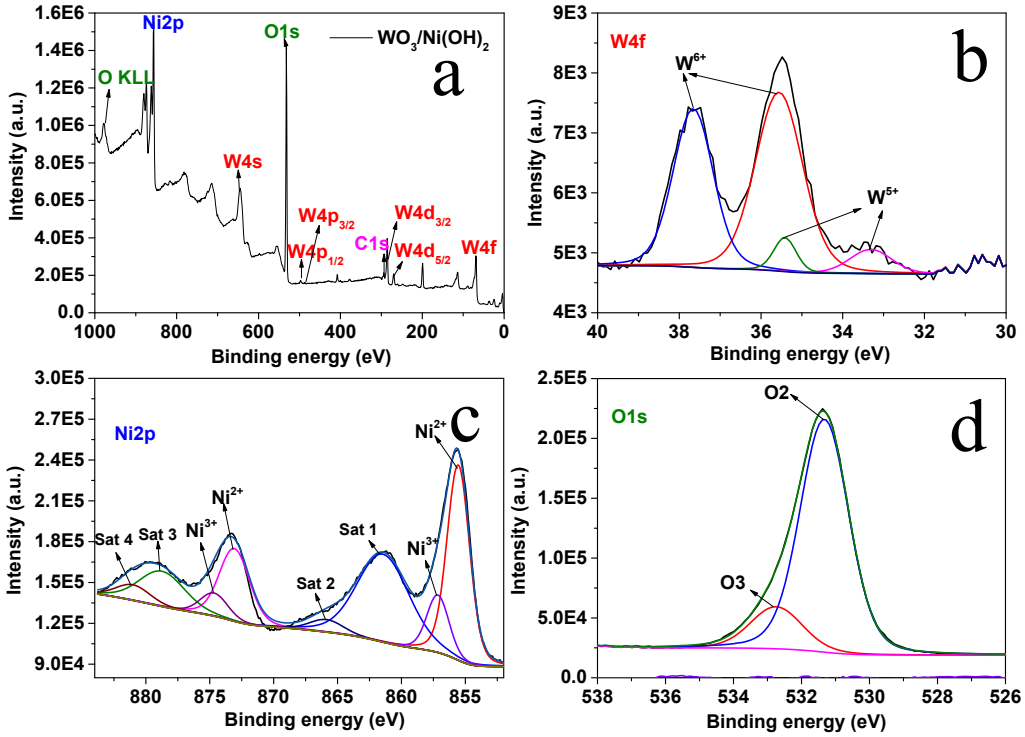

Figure S5: (a) XPS survey spectrum of $WO_3/Ni(OH)_2$, high-resolution XPS spectra of (b) W 4f, (c) Ni 2p, and (d) O 1s.

Supporting Information

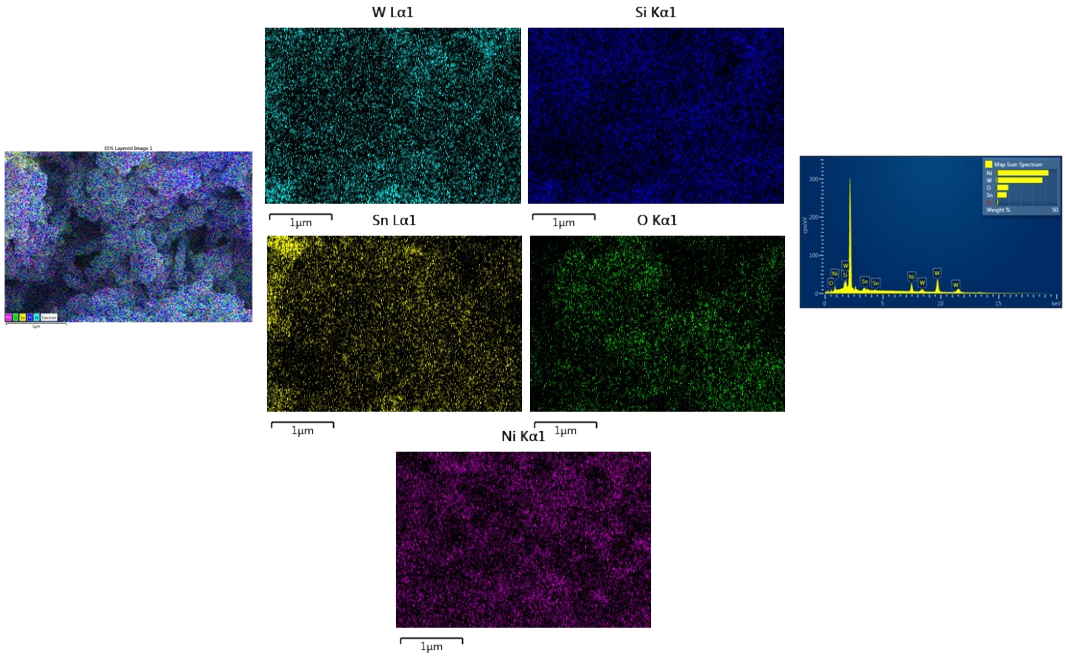

Map Sum Spectrum	Atomic %
O	37
Si	3
Ni	44
Sn	4
W	12
Total	100.00

Figure S6: EDS mapping analysis of WO_3/NiOOH indicating the presence of W, Ni, and O as elements.

.

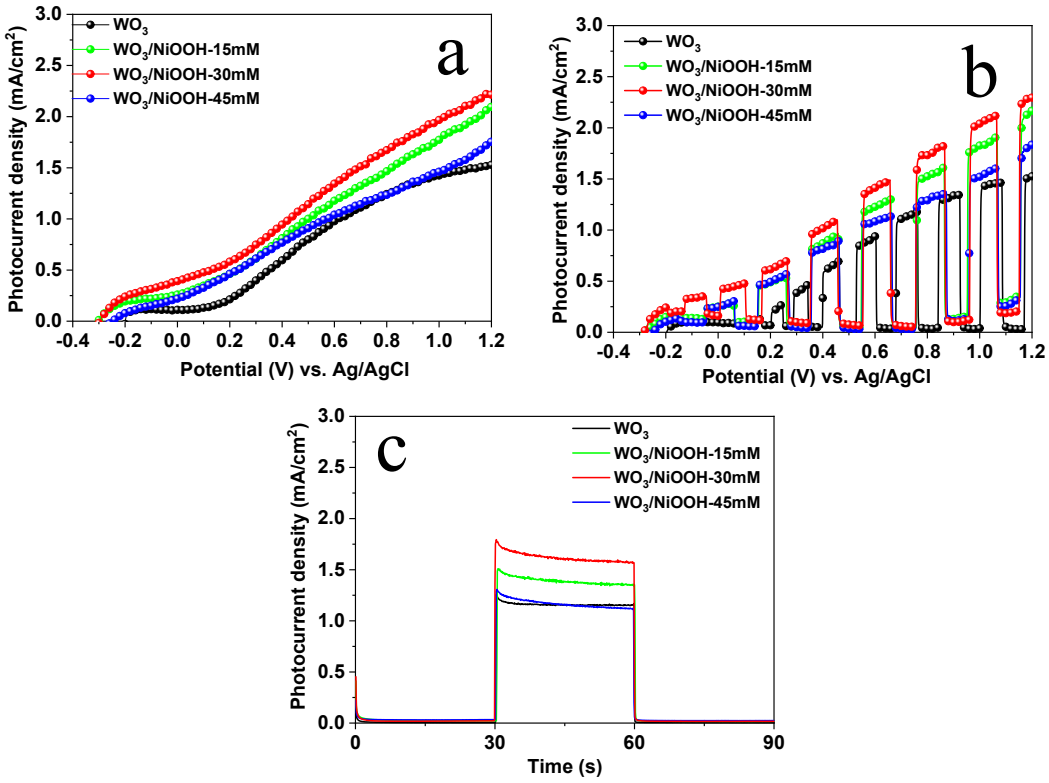

Figure S7: LSV curve showing variation in photocurrent density with applied potential under (a) continuous, (b) chopped illumination condition, (c) *i-t* plot of WO_3, WO_3/NiOOH-15mM, WO_3/NiOOH-30mM, and WO_3/NiOOH-45mM, at fixed potential of 0.8 V vs. Ag/AgCl observed for 90 seconds.

Supporting Information

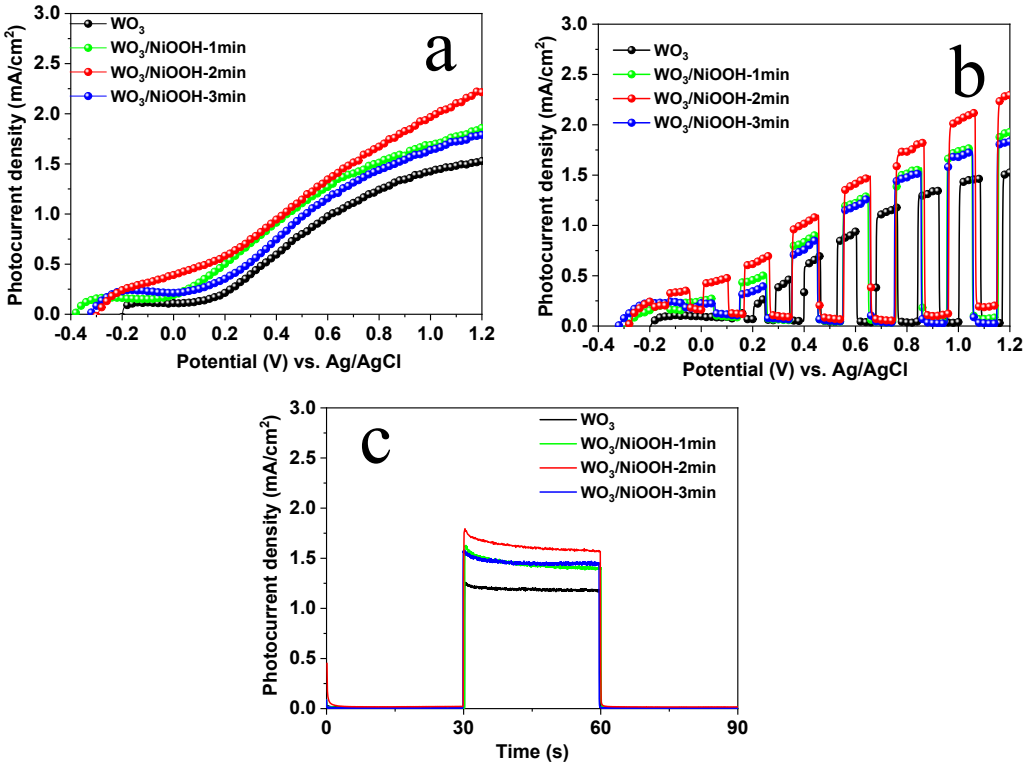

Figure S8: LSV curve showing variation in photocurrent density with applied potential under (a) continuous, (b) chopped illumination condition, (c) *i-t* plot of WO_3, WO_3/NiOOH-1min, WO_3/NiOOH-2min, and WO_3/NiOOH-3min, at fixed potential of 0.8 V vs. Ag/AgCl observed for 90 seconds.

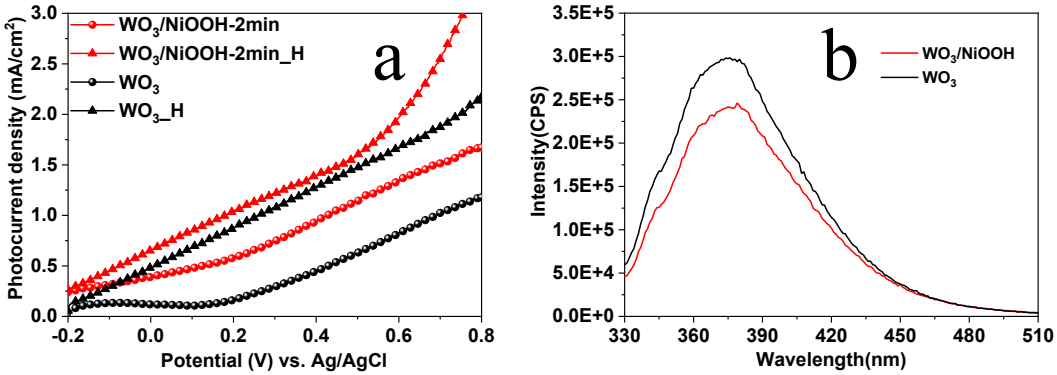

Figure S9: Comparative photocurrent density of WO_3 and WO_3/NiOOH in 3.5wt% aqueous solution of NaCl and 3.5wt% aqueous solution of NaCl along with 0.5M Na_2SO_3 as the hole scavengers, and (b) Steady state photoluminescence spectra of WO_3 and WO_3/NiOOH.

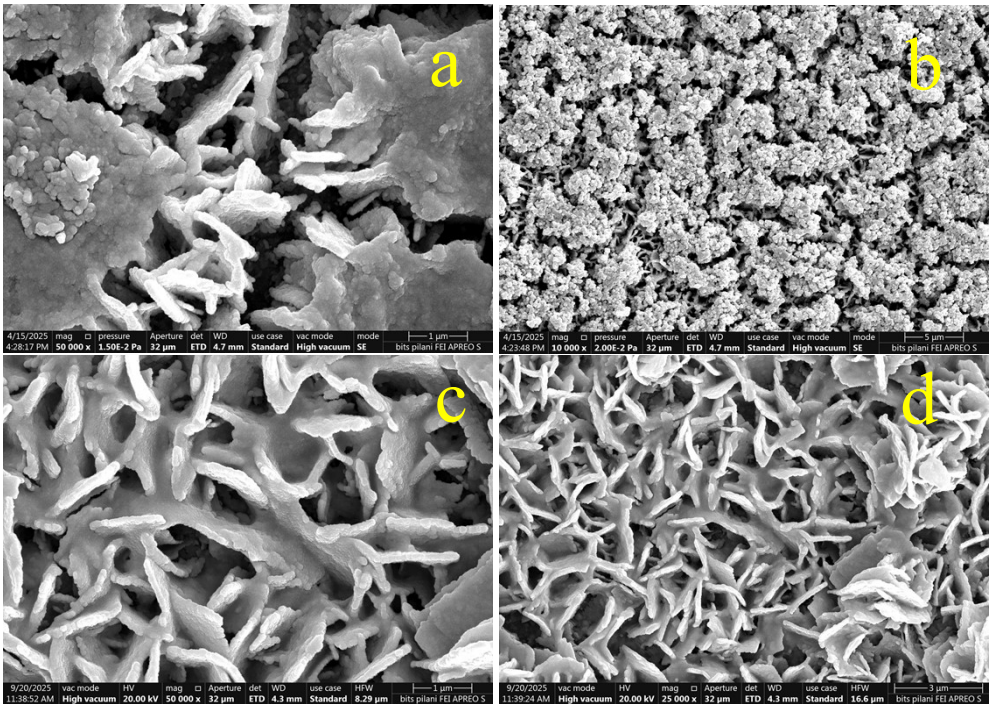

Figure S10: FESEM images of WO_3/NiOOH after (a-b) 1 h and (c-d) 5 h of photostability test, in different magnifications

Supporting Information

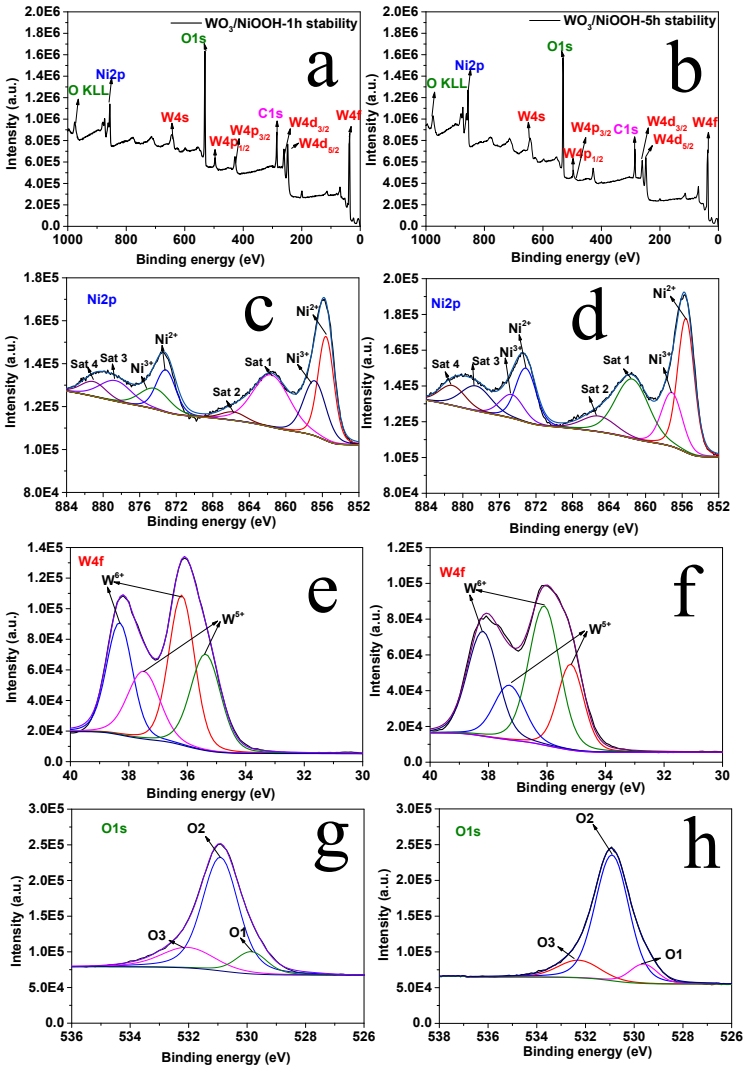

Figure S11: (a-b) XPS survey spectrum of WO_3/NiOOH after photostability test of 1h and 5 h, respectively, high-resolution XPS spectra of Ni 2p (c-d), W 4f (e-f), and O 1s (g-h) after photostability test of 1h (left) and 5 h (right), respectively.

Supporting Information

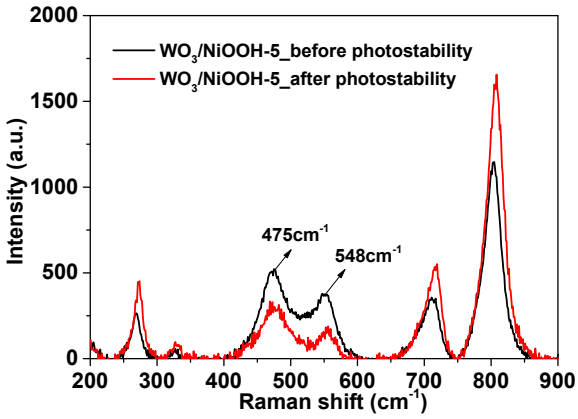

Figure S12: Raman spectra of WO_3/NiOOH before and after photostability test.

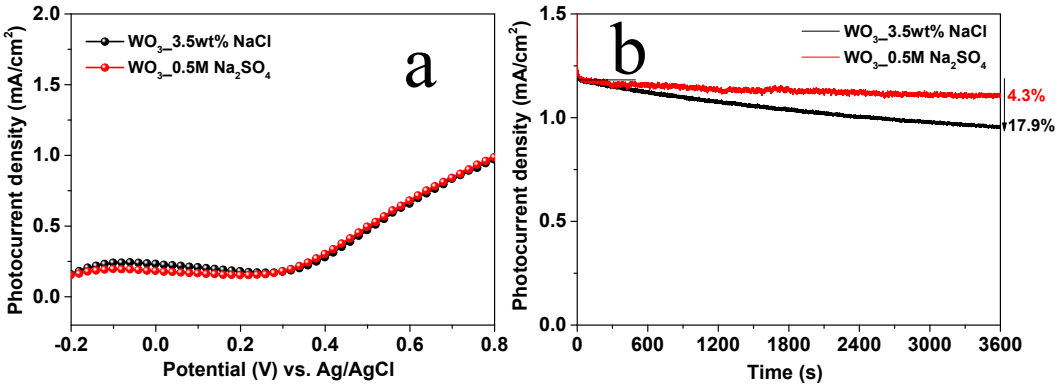

Figure S13: Comparative (a) LSV curve showing variation in photocurrent density with applied potential under continuous illuminations and (b) *i-t* plot of WO_3 at fixed potential of 0.8 V vs. Ag/AgCl observed for 3600 seconds in 3.5 wt% NaCl and 0.5 M Na_2SO_4 electrolytes.

Supporting Information

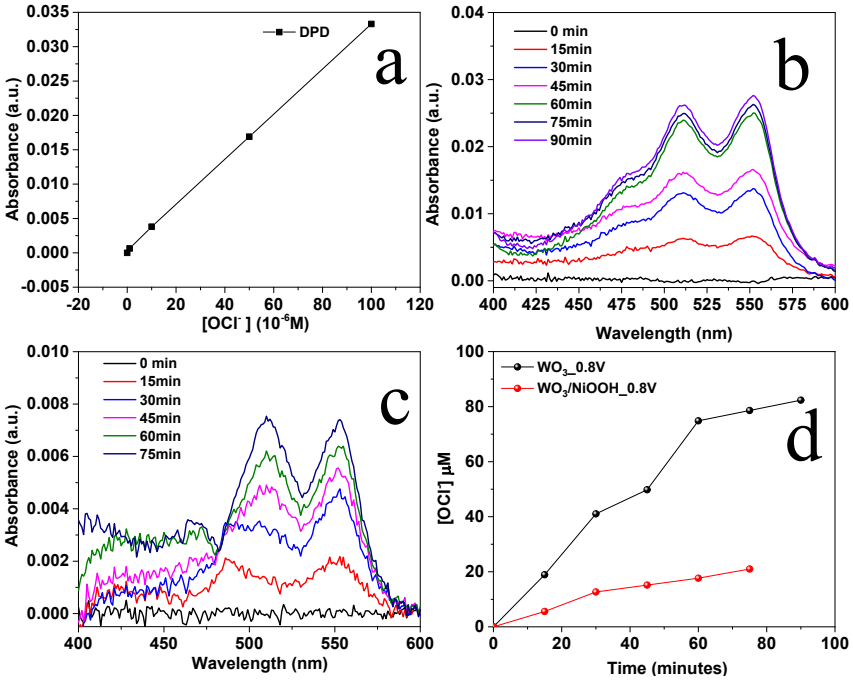

Figure S14: (a) The calibration curve for DPD colorimetric analysis at different concentrations of OCl^-, DPD absorbance of (b) WO_3 and (c) WO_3/NiOOH-5 for different amperometry (i-t) timings at 0.8 V vs. Ag/AgCl, and (d) OCl^- concentration variations with time for WO_3 and WO_3/NiOOH-5 at 0.8 V vs. Ag/AgCl.

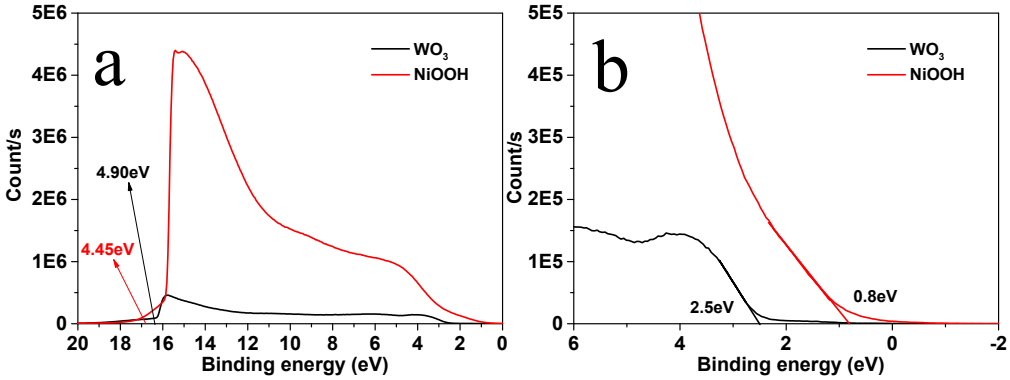

Figure S15: UPS spectra of WO_3 and NiOOH

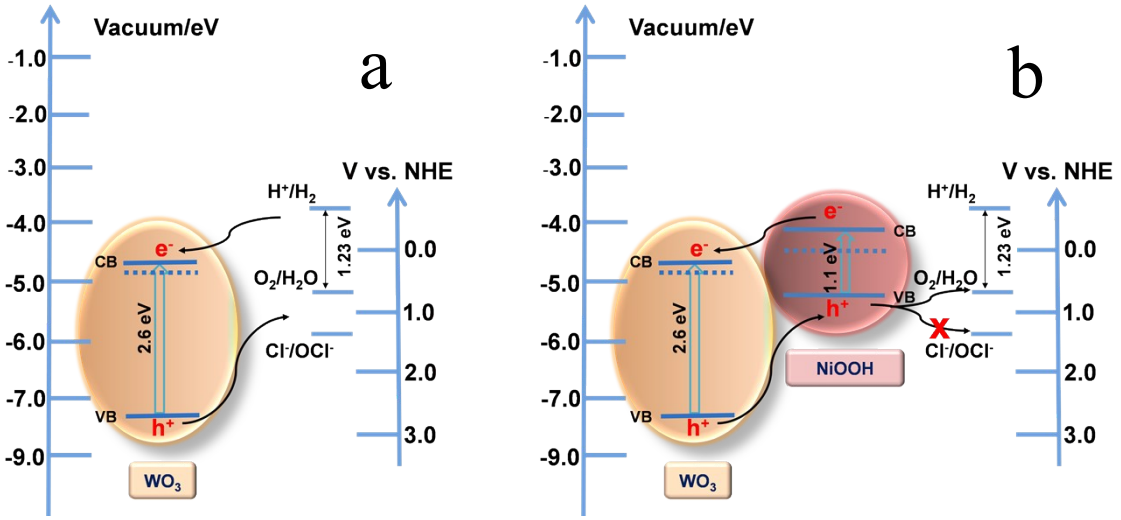

Figure S16: Band alignment of (a) WO_3 and (b) WO_3/NiOOH with respect to water and chloride ion oxidation potential, which indicates that on the surface of WO_3, Cl^- oxidation is competing with water oxidation, whereas on the WO_3/NiOOH surface, only water oxidation is favoured (arrows indicate the direction of hole and electron migration).

Supporting Information

Table S1a: Rietveld refinement parameters for WO_3

Parameter	**Symbol**	**Refined value**
Lattice constant	a	7.30
Lattice constant	b	7.51
Lattice constant	c	7.67
Angle	□	90.59°
Weighted profile R-factor	R_{wp}	9.17
Profile R-factor	R_p	6.97
Goodness of fit	χ^2	2.22

Table S1b: Rietveld refinement parameters for WO_3/NiOOH

Parameter	**Symbol**	**Refined value**
Lattice constant	a	7.33
Lattice constant	b	7.50
Lattice constant	c	7.65
Angle	□	90.27°
Weighted profile R-factor	R_{wp}	5.57
Profile R-factor	R_p	4.43
Goodness of fit	χ^2	1.28

Table S2:

S.N.	Photoanodes	Morphology	Electrolyte	Photocurrent density	References
1	WO_3/FeOOH	Flower-like morphology of FeOOH on WO_3 nanoplates	0.1 M Na_2SO_4	2.63 mA/cm^2 at 1.23 V *vs.* RHE	1
2	(FeNiCo)OOH/WO_3 /W	Nanoplates	0.5 M NaCl solution	4.85 mA/cm^2 at 1.23 V vs. RHE	2
3	F:FeOOH/$BiVO_4$/WO_3	Core-shell structure	0.1 M KPi buffer solution	3.1 mA/cm^2 at 1.23 V (*vs.* RHE)	3
4	WO_3/CdS/NiOOH/Co-Pi	Nanoparticles on nanorods	0.2 M Na_2SO_4	2.59 mA/cm^2 at 1.0 V vs RHE	4
5	WO_3/C_3N_4/CoOx	Nanoparticles on nanosheets	0.01 M Na_2SO_4	5.76 mA/cm^2 at 2.1 V vs. RHE	5
6	(WO_3/$BiVO_4$)-OV/CoPi	Nanoflakes	0.1 M Na_2SO_4 and 0.1 M KPi	2.9 mA/cm^2 at 1.6 V vs. RHE	6
7	WO_3/Fe_2O_3/NiFe-LDH	NiFeLDH sheets on WO_3/Fe_2O_3	1 M NaOH	3.0 mA/cm^2 at 0.8 V vs Ag/AgCl	7
8	α-Fe_2O_3@NiOOH	Nanosheets	1 M NaOH	626.137 μA/cm^2 at 1.23 V (vs. RHE)	8
9	GaP/NiOOH	Nanoparticles	0.5 M H_2SO_4	1.15 mA/cm^2 at 0.5V vs Ag/AgCl	9
10	$BiVO_4$/CoFe-NiOOH	Nanoworms	0.5 M Na_2SO_4	1.54 mA/cm^2 at 1.23 V vs (RHE)	10
11	WO_3/SNCDs	2D nanosheets	3.5 wt% NaCl	2.57 mA/cm^2 at 1.39 V vs Ag/AgCl	11
12	WO_3/$ZnWO_4$	Nanoflakes	3.5 wt% NaCl	2.30 mA/cm^2 at 1.2 V vs Ag/AgCl	12
13	Ag/WO_3/ZnFe-LDH	Nanoplates	Natural seawater	1.18 mA/cm^2 at 1.23 V vs the RHE	13
14	Defect-rich WO_3	Thin films	0.5 M NaCl	0.66 mA/cm^2 at 1.50 V vs Ag/AgCl	14
15	Stacked WO_3 array	Plates	0.5 M NaCl	1.7 mA/cm^2 at 0.6 V vs Ag/AgCl	15
16	WO_3/NiOOH	Nanoflakes	3.5 wt% NaCl	2.23 mA/cm^2 at 1.2 V vs Ag/AgCl	This study

REFERENCES:

1. G. Zheng, S. Jiang, M. Cai, F. Zhang and H. Yu, *J. Alloys Compd.*, 2024, **981**, 173637.
2. M. Saeidi, Z. Z. Faradonbeh, K. Rahimi, A. Z. Moshfegh, J. Bai and A. Simchi, *Appl. Catal. B: Environ.*, 2025, **362**, 124778.

3. Y. Li, Q. Mei, Z. Liu, X. Hu, Z. Zhou, J. Huang, B. Bai, H. Liu, F. Ding and Q. Wang, *Appl. Catal. B: Environ.*, 2022, **304**, 120995.
4. Y. Li, Z. Liu, J. Zhang, Z. Guo, Y. Xin and L. Zhao, *J. Alloys Compd.*, 2019, **790**, 493-501.
5. Y. Hou, F. Zuo, A. P. Dagg, J. Liu and P. Feng, *Adv. Mater.* 2014, **26**, 5043-5049.
6. J. Liu, W. Chen, Q. Sun, Y. Zhang, X. Li, J. Wang, C. Wang, Y. Yu, L. Wang and X. Yu, *ACS Appl. Energy Mater.*, 2021, **4**, 2864-2872.
7. S. Bai, X. Yang, C. Liu, X. Xiang, R. Luo, J. He and A. Chen, *ACS Sustain. Chem. Eng.*, 2018, **6**, 12906-12913.
8. P. Qiu, F. Li, H. Zhang, S. Wang, Z. Jiang and Y. Chen, *Electrochim. Acta.*, 2020, **358**, 136847.
9. I. V. Bagal, M. Arunachalam, A. Waseem, A. Abdullah, S. H. Kang and S.-W. Ryu, *Appl. Surf. Sci.*, 2021, **558**, 149873.
10. G. Fang, Z. Liu, C. Han, P. Wang, X. Ma, H. Lv, C. Huang, Z. Cheng and Z. Tong, *ACS Appl. Energy Mater.*, 2021, **4**, 3842-3850.
11. P. Choubey, M. D. Sharma and M. Basu, *ACS Appl. Nano Mater.*, 2024, **7**, 18251-18261.
12. P. Choubey, R. Verma and M. Basu, *Chem. Asian J.*, 2025, **20**, e202500292.
13. J. Liu, S.-M. Xu, Y. Li, R. Zhang and M. Shao, *Appl. Catal. B-Environ.*, 2020, **264**, 118540.
14. J. O'Hara, N. S. Thabit, H. Chrenka, L. I. Vogt, J. E. Penner Hahn, C. P. Woodley and B. M. Bartlett, *ACS Appl. Energy Mater.*, 2025, **8**, 12749-12759.
15. S. Y. Jo, J. Y. Bae, J. Y. Park, M. K. Kim, W.-S. Chae, Y.-I. Kim and K. M. Nam, *ACS Appl. Mater. Interfaces.*, 2024, **16**, 54864-54872.